

# Size Effects on the Interaction of QDs with the Mitochondrial Membrane In Vitro

Lu Lai<sup>1</sup> · Ya-Ping Li<sup>1</sup> · Ping Mei<sup>1</sup> · Wu Chen<sup>1</sup> · Feng-Lei Jiang<sup>2</sup> · Yi Liu<sup>2</sup>

Received: 21 April 2016 / Accepted: 1 August 2016 / Published online: 10 August 2016  
© Springer Science+Business Media New York 2016

**Abstract** The mitochondrial toxicity induced by GSH-CdTe Quantum dots (QDs) of different sizes was investigated. The decreases in absorbance and transmission electron microscopy images show that QDs induce the swelling of mitochondria. Results of flow cytometry indicate that QDs cause a reduction of mitochondrial membrane potential (MMP). A remarkable increase in fluidity of protein regions of mitochondrial membrane is observed, whereas the lipid regions are not obviously affected. Cyclosporin A (CsA) effectively prevents the QD-induced mitochondrial swelling. On the basis of these results, it is proposed that QDs induce mitochondrial permeability transition (MPT). Moreover, with increasing QDs size, a pronounced MPT is observed. The difference between the membrane fluidity induced by QDs and Cadmium ion and the ineffective protective effects of EDTA suggests that the mitochondrial toxicity of QDs cannot be only attributed to the release of metal ion. The protective effects of HSA indicate that the interaction of QDs with pore-forming

protein gives rise to the increase in membrane fluidity. This hypothesis is demonstrated by the interaction of QDs with model membranes and proteins using differential scanning calorimetry and isothermal titration microcalorimetry. In conclusion, as the size of QDs increases, the binding affinity of QDs with membrane protein increases, and therefore causes a pronounced mitochondrial damage.

**Keywords** CdTe Quantum dots · Mitochondria · Model membranes

## Introduction

QDs are nanocrystal synthesized from semiconductor materials, such as CdS, CdTe, CdSe, ZnS, etc., which is small (from 2 to 10 nm in diameter) enough to exhibit quantum confinement (Leutwyler et al. 1996). Due to their high extinction coefficient, QDs exhibit extraordinary optical properties, including tunable fluorescence emission, wide excitation spectra, narrow emission spectra, and resistant to photobleaching (Michalet et al. 2005). Because of their excellent optical properties, QDs are of interest in many research fields such as transistors (Choi et al. 1998), solar cells (Raffaella et al. 2002), LEDs (Son et al. 2012), diode lasers (Eliseev et al. 2000), medical imaging (Kim et al. 2004), and quantum computing (Loss and DiVincenzo 1998).

Despite the invaluable potential applications of QDs, current studies demonstrate that some QDs pose potential threats to human health and environment (Chen et al. 2012; Hardman, 2006). So far, the toxicity of QDs has been extensively investigated at the different levels, including protozoa (Werlin et al. 2011), cell (Lai et al. 2015b; Su et al. 2009), subcellular organelles (Lai et al. 2015a), biological macromolecules (Xiao et al. 2012), and others

**Electronic supplementary material** The online version of this article (doi:10.1007/s00232-016-9920-3) contains supplementary material, which is available to authorized users.

✉ Lu Lai  
lailu@aliyun.com

✉ Yi Liu  
yiliu@whu.edu.cn

<sup>1</sup> College of Chemistry and Environmental Engineering, Yangtze University, Jingzhou 434023, People's Republic of China

<sup>2</sup> State Key Laboratory of Virology and Key Laboratory of Analytical Chemistry for Biology and Medicine (Ministry of Education), College of Chemistry and Molecule Sciences, Wuhan University, Wuhan 430072, People's Republic of China

(Yang et al. 2014). However, most studies have focused on the mechanism of QDs cytotoxicity using different cell lines.

Mitochondria are a double membrane-bound organelle. The diameter of mitochondria ranges from 0.5 to 1.0  $\mu\text{m}$ . As the power plants of cell, mitochondria also play a vital role in cell death through apoptosis, necrosis, or autophagy (Balaban et al. 2005). Mitochondrial permeability transition (MPT) is an increase in the permeability of the mitochondrial membranes, which is characterized by the opening of a non-specific MPT pore (MPTP) (Lemasters et al. 2009). MPT causes the mitochondrial swelling, the depolarization of the mitochondrial, and cell apoptosis or necrosis (Kowaltowski et al. 2001).

Besides the cell membrane, Unfried et al. indicated that cell nucleus and mitochondria are key organelle relevant for possible cytotoxicity induced by nanoparticles (Unfried et al. 2007). In recent years, more studies have proposed that mitochondria are relevant targets in nanoparticle-induced cytotoxicity (Piao et al. 2011; Sharma et al. 2012). For example, Xin et al. reported that the cytotoxicity induced by AgNPs may result from mitochondrial injury (Xin et al. 2015). Nalika et al. also demonstrated that titanium dioxide nanoparticles may exhibit a health risk to mitochondria with the generation of ROS (Nalika and Parvez 2015). However, most published studies on the toxicity related to nanoparticles have concerned about the mitochondrial damage in different cell lines. Results of direct and immediate effects of nanoparticles on mitochondrial dysfunction are still rather scarce. Meanwhile, the mechanisms by which nanoparticles interact with mitochondria and affect their functions are unknown. Consequently, further research is urgently required on the mechanism of nanoparticle-induced mitochondrial damage. Our group examined the damage of QDs on mitochondria isolated from rat liver, and first proposed that mitochondria is a key target of QD-induced toxicity (Li et al. 2011). The size and the surface physicochemical property of nanoparticles are always considered as two major factors relevant for nanoparticle-induced toxicity (Liu et al. 2010; Schleh et al. 2012). We have already investigated the mitochondrial damage of CdTe QDs with different surface coatings (Lai et al. 2015a). In this report, the mitochondrial toxicity of CdTe QDs of different sizes was examined using spectroscopic methods and flow cytometry. On the basis of experiment results, the interaction of QDs with model membranes and proteins was also performed using differential scanning calorimetry and isothermal titration microcalorimetry. Results of our research are conducive for understanding the possible mechanism of mitochondrial damage related to nanoparticles.

## Experimental Section

### Materials

Tellurium powder (about 200 mesh, 99.999 %), reduced L-glutathione (GSH, 98 %),  $\text{CdCl}_2$  (99.99 %), cyclosporin A (CsA), human serum albumin (HSA),  $\text{NaBH}_4$  (99 %), and hematoporphyrin (HP) were purchased from Sigma-Aldrich. MMP detection kit (JC-1) was obtained from MultiSciences Biotech Co., Ltd. (China). 3-(4, 5-dimethylthiazolyl-2)-2, 5-diphenyltetrazolium bromide (MTT) was obtained from Aladdin (China). Dipalmitoylphosphatidylcholine (DPPC, 99 %) was purchased from Avanti Polar Lipid (Alabaster, USA). All other reagents used were of analytical reagent grade. Ultrapure water used as solvent in all experiments was produced using a Milli-Q apparatus (resistivity 18.2  $\text{M}\Omega\text{-cm}$ ).

### Cell Culture and Treatment Conditions

Human embryonic kidney cells (HEK 293) were maintained at 37 °C (5 %  $\text{CO}_2$ ) in DMEM medium (Gibco, Canada) containing 10 % fetal bovine serum. All media contained penicillin and streptomycin. For biochemical analysis and cell imaging, HEK 293 cells were seeded in 6-well plates or 96-well plates (Corning, US) at a density of  $4.0 \times 10^5$  cells/ $\text{cm}^2$ . Then, GSH-CdTe QDs of different sizes were added to cells for 24 or 48 h.

### Assessment of HEK293 Cell Metabolic Activity

The effects of QDs on the metabolic activity of HEK293 cells were examined by MTT assays. The cells were cultured in 96-well plates (200  $\mu\text{L}$ /well). After 24 h treatment, different concentrations of GSH-CdTe QDs of different sizes were added to each well. Then, the culture medium was discarded and replaced by PBS solution (180  $\mu\text{L}$ /well) after 48-h treatment. To each well, aliquots of 20  $\mu\text{L}$  MTT solution (5 mg/mL) was added and incubated with HEK 293 cells for 4 h. Following incubation the buffer was discarded, and cells were treated with DMSO (dimethylsulfoxide). A490 values were detected using a BioTek microplate reader (Elx800, USA). Compared with the A490 value of QD-free group, relative cell viability was determined.

### Isolation of Liver Mitochondria

According to the standard procedures provided by Zhang et al. (2011), the active liver mitochondria were isolated from Wistar rats (about 150 g).

### Determination of MMP ( $\Delta\psi_m$ )

To detect the  $\Delta\psi_m$  changes, the fluorescent lipophilic cationic probe JC-1 was used. JC-1 shows a potential-dependent accumulation into the mitochondrial matrix. When mitochondrial membrane potential decreases, the maximum emission wavelength of JC-1 shifts from  $\sim 590$  to  $\sim 525$  nm. Therefore, the loss of  $\Delta\psi_m$  was examined using flow cytometry. The fluorescence of JC-1 aggregates in healthy cells and JC-1 monomers in apoptotic cells was determined on PE detector and FITC detector of BD flow cytometer (FACS Aria<sup>TM</sup> III, USA), respectively. For statistical analysis, at least 10,000 HEK 293 cells were examined in each sample.

### Evaluation of Mitochondrial Swelling

According to reference (Bernardi et al. 1992), the swelling of mitochondria was monitored on the change in absorbance at 600 nm in the mitochondrial suspension at room temperature. The procedure is as follows. Isolated rat liver mitochondria (0.25 mg/mL) were dispersed in 2 mL buffer (200 mM sucrose, 20  $\mu$ M EGTA-Tris, 10 mM Tris-MOPS, 2  $\mu$ M rotenone, 5 mM succinate, and 3  $\mu$ g/mL oligomycin, pH 7.4), and treated with different concentrations of GSH-QDs. The change in absorbance at 600 nm was detected on a spectrophotometer (TU-1901, Puxi Analytic Instrument Ltd., China).

### Determination of Inner Mitochondrial Membrane (IMM) Permeabilization to $H^+$ and $K^+$

The inner membrane permeabilization of rat liver mitochondria to  $H^+$  and  $K^+$  was determined following the method described elsewhere (Fernandes et al. 2006). The potassium acetate buffer contained 135 mM KAc, 0.2 mM EDTA, 0.1 mM EGTA, 2  $\mu$ M rotenone, 5 mM HEPES, and 1  $\mu$ g/mL valinomycin (pH 7.1). The potassium nitrate buffer contained 135 mM  $KNO_3$ , 5 mM HEPES, 0.2 mM EDTA, 0.1 mM EGTA, and 2  $\mu$ M rotenone (pH 7.1).

### Measurement of Membrane Fluidity

According to published procedures (Ricchelli et al. 2005), the membrane fluidity of isolated mitochondria was detected by anisotropy changes of DPH-labeled and HP-labeled mitochondria.

### Transmission Electron Microscopy of Cell

Control cells and QD-treated cells were fixed in 2.5 % glutaraldehyde in 0.1 M sodium cacodylate buffer for 30 min at 4 °C, then post fixed in osmium tetroxide (1 %

and dehydrated for a minimum of 1 h (Petronilli et al. 2009). TEM images were obtained using a transmission electron microscope (JEM-100CX, JEOL).

### Differential Scanning Calorimetry (DSC)

DPPC was dissolved in chloroform to a final concentration of 1 mM. The DPPC solution was evaporated using a rotary evaporator under reduced pressure. The resulting DPPC films were dried under vacuum at 25 °C, and then hydrated with 5 mL ultrapure water for 1 h at 50 °C. To obtain multilamellar vesicles (MLV), the suspensions were sonicated at room temperature. Large unilamellar vesicles (LUV) were prepared by extruding the MLV suspensions ten times through a 0.1- $\mu$ m polycarbonate membrane using a LipoFast extrusion apparatus (Avestin Inc.) at 55 °C.

The temperature of the phase transition of DPPC solutions was determined using a Nano Differential Scanning Calorimeter (TA, USA). All reference and sample solutions were degassed prior to being placed in the DSC. These solutions were cooled to 10 °C and then heated to 70 °C. The heating rate was 1 °C/min. The maximum temperature of the main phase transition was determined using NanoAnalyze software provided by TA Instruments.

### Isothermal Titration Microcalorimetry (ITC)

A Nano-ITC<sup>2G</sup> isothermal titration microcalorimeter (TA, USA) with a 1-mL sample cell was used in this work. The isothermal titration was carried out as an incremental titration with a 250- $\mu$ L syringe and a 1-mL cell. All the experiments were performed at 298.15 K. The stir speed was set to 150 rpm. The time settings were as follows: injection interval: 600 s; data interval: 1.0 s; initial baseline: 1800 s; and start delay: 1800 s. The injection number was 50, while the injection volume was set as 5  $\mu$ L. The control experiment was carried out under the same conditions, using the DPPC solution or HSA solution as titrant and PBS buffer solution as the titrand. Subtracting the control experiment gave the corrected heat power for each injection. The baseline of titration was manually set and then the peak area was analyzed by NanoAnalyze software (TA Instruments).

## Results

### Characterization of GSH-CdTe QDs with Different Sizes

Green-emitting QDs (GQDs), orange-emitting QDs (OQDs), and red-emitting QDs (RQDs) are synthesized at different reflux times. With increasing the particle sizes,

the maximum emission wavelength of QDs shifts to a longer wavelength. Figure 1 shows the UV-vis and PL spectra of these three QDs at room temperature. The maximum emission wavelengths of these three QDs are at 522, 570, and 621 nm, respectively. The image of these QDs water dispersion under UV lamp radiation is shown in the inset of Fig. 1. In order to examine the hydrodynamic radii of QDs, dynamic light scattering experiments were performed. The results show that the hydrodynamic diameters of green-emitting QDs (GQDs), orange-emitting QDs (OQDs), and red-emitting QDs (RQDs) are  $5.22 \pm 0.17$ ,  $7.21 \pm 0.19$ , and  $9.34 \pm 0.37$  nm, respectively. The polydispersity indexes for the hydrodynamic diameters of GQDs, OQDs, and RQDs are  $0.08 \pm 0.04$ ,  $0.11 \pm 0.05$ , and  $0.13 \pm 0.06$ , respectively (The size determination of QDs was performed using three independent experiments). In addition, the powder X-ray diffraction patterns and X-ray photoelectron spectra of GQDs are shown in Figs. S1 and S2, respectively.

### Cytotoxicity of Differently Sized GSH-CdTe QDs

The cytotoxicity of GSH-CdTe QDs was examined through MTT assay. As shown in Fig. 2, with increasing the QDs concentration, the cell metabolic activity decreases. In addition, RQDs are significantly more toxic than GQDs and OQDs in the concentration range from 100 to 2400 nM. The cytotoxicity of QDs increases with increasing QDs size. Therefore, there seems to be a relationship between the cytotoxicity and size of GSH-CdTe QDs.

### Effects of Differently Sized QDs on MMP

Opening of permeability transition pores initiates MPT. During this process, a collapse in the mitochondrial membrane potential will be observed. JC-1 is widely used

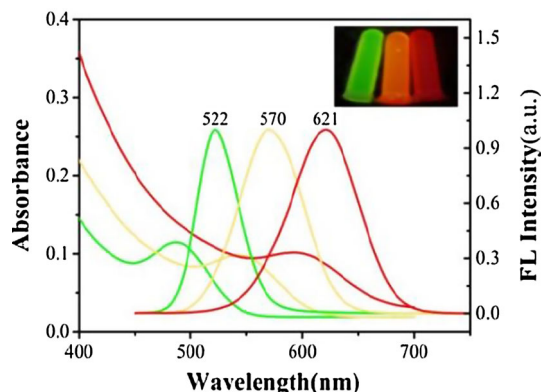


**Fig. 1** Absorption and corrected emission spectra of differently sized GSH-CdTe QDs (GQDs, OQDs, and RQDs) in water

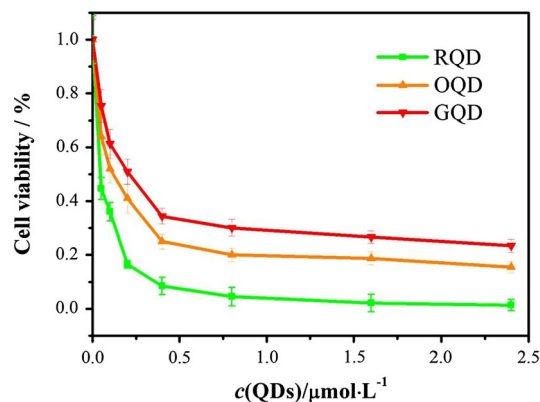


**Fig. 2** Effects of differently sized GSH-CdTe QDs (GQD, OQD, and RQD) on cell viability determined by MTT assay. HEK293 cells were incubated with different doses of GSH-CdTe QDs for 48 h. Error bars represent standard errors of the mean values. This experiment was performed using four independent experiments with different cell preparations

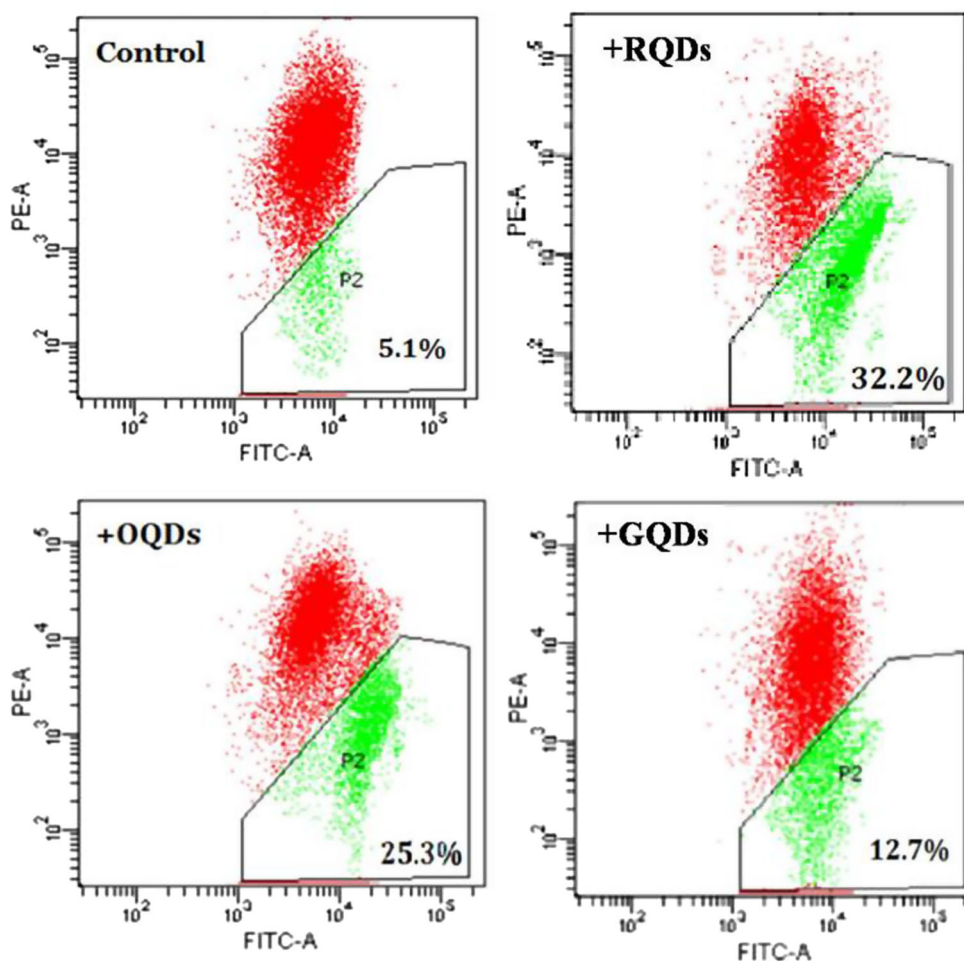
to determine the mitochondrial depolarization. The normal mitochondria are stained with JC-1 probes and display the bright red emission. When MMP collapses in apoptotic cells, probes emit green fluorescence (Cossarizza et al. 1993). Consequently, the mitochondrial depolarization is signed by a decrease in the ratio of the red/green emission intensity.

As shown in Fig. 3, the effects of differently sized QDs on MMP are revealed using JC-1 probes. With the addition of QDs, an increased cell number in P2 gate are observed. A decrease in the intensity of red fluorescence indicates the loss of MMP. In Fig. 3, RQDs induce a remarkable decrease in MMP, as the percentage of HEK293 cells falling into P2 gate increases from 5.1 to 32.2 in the presence of 200 nM RQDs. Compared with RQDs, the percentage of HEK293 cells of low  $\Delta\psi_m$  increases to 25.3 and 12.7 with the addition of OQDs and GQDs, respectively. Therefore, with decreasing the QDs size, QDs show less effect on MMP.

### Mitochondrial Swelling Induced by QDs

It is reported that the opening of MPT pore gives rise to the mitochondrial depolarization and swelling (Kim et al. 2003). In order to reveal the effect of exposure of mitochondria to differently sized QDs on MPT, we monitored the mitochondrial swelling induced by QDs. As shown in Fig. 4a, the representative decrease in A600 after the addition of RQDs indicates that RQDs cause mitochondrial swelling. With increasing QDs concentration, the value of A600 decreases with significant dose-effect relationship. Moreover, the swelling induced by RQD is most pronounced and followed by OQD, whereas the swelling induced by GQD is the weakest (Fig. 4b). In addition, the

**Fig. 3** Effects of differently sized GSH-CdTe QDs (GQD, OQD, and RQD) on mitochondrial membrane potential. HEK293 cells were incubated with  $200 \text{ nmol}\cdot\text{L}^{-1}$  of QDs for 24 h, and then stained with JC-1. The red fluorescence of J-aggregates in healthy cells was quantified on PE detector, and green JC-1 monomers in apoptotic cells were quantified on FITC detector of flow cytometer. Records are representative of four experiments obtained from different cell preparations



morphological changes of HEK 293 cells induced by QDs were observed using TEM. The TEM images exhibit that QDs induce the morphological alternation of mitochondria, including the expansion of the volume and intermembrane space. Meanwhile, many clusters of the cristae are observed (Fig. 4c).

### Permeabilization of Inner Mitochondrial Membrane (IMM) Induced by QDs

Permeabilization of IMM to  $\text{H}^+$  is measured by monitoring the mitochondrial swelling in KAc medium (Liu et al. 2011). HAc passes through the IMM and dissociates into the  $\text{Ac}^-$  and  $\text{H}^+$  in the mitochondrial matrix, thus producing a proton gradient. A valinomycin-dependent swelling can only be observed in the absence of the proton gradient (Bernardi et al. 1992). Consequently, the decrease in A600 is monitored, which exhibits the changes in permeabilization of IMM to  $\text{H}^+$  resulted from the addition of QDs.

As shown in Fig. 5a, a little swelling is observed for the QD-free mitochondria. After the addition of QDs, the

permeabilization of IMM to  $\text{H}^+$  obviously increases. Furthermore, RQDs induce permeabilization of IMM to  $\text{H}^+$  in a dose-effect manner. Figure 5b shows the difference in the permeabilization of IMM to  $\text{H}^+$  caused by differently sized QDs. The permeabilization of IMM has the greatest sensitivity to the addition of RQDs. As the size of QDs decreases, the changes in the permeabilization of IMM are depressed.

Permeabilization of IMM to  $\text{K}^+$  is evaluated by monitoring the mitochondrial swelling in  $\text{KNO}_3$  medium (Liu et al. 2011). The addition of RQDs leads to an obvious swelling of mitochondria (Fig. 5c). As shown in Fig. 5d, the effects of differently sized QDs on the permeabilization of IMM to  $\text{K}^+$  are similar to those on the permeabilization of IMM to  $\text{H}^+$ .

### The Changes in Membrane Fluidity Induced by QDs

The induction of MPT gives rise to the changes in fluidity of mitochondrial membranes (Ricchelli et al. 2005). The change of fluorescence anisotropy of mitochondria-bound probes is used to determine the fluidity changes of

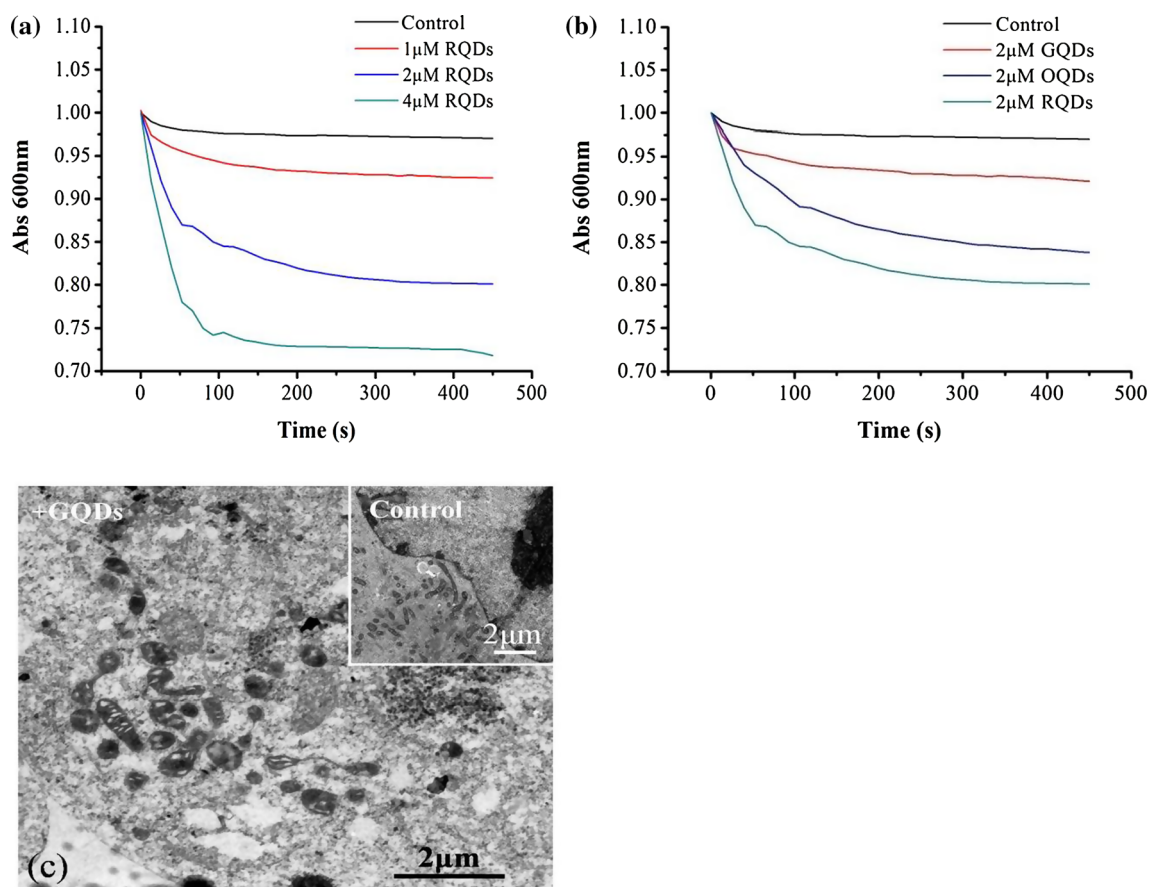


**Fig. 4** QDs induced mitochondrial swelling. Mitochondrial swelling was measured by monitoring the decrease of absorbance at 600 nm at room temperature. **a** Mitochondria incubated with different concentrations of RQDs: 0, 1, 2 and 4  $\mu\text{mol}\cdot\text{L}^{-1}$ . **b** Mitochondria incubated with differently sized GSH-CdTe QDs: GQDs, OQDs and RQDs. **c** The GQDs-induced mitochondrial swelling observed by

transmission electron microscopy. The image of untreated mitochondria is shown in the inset of Fig. 4c). The determination of mitochondrial swelling was performed using four independent experiments with different mitochondria preparations. The mean values and *standard errors* are shown in Figs. S3 and S4

mitochondrial membranes. Here, we have examined the changes in anisotropy of DPH and HP. It was proved that HP mainly accumulates in polar regions or associates with proteins in the mitochondrial membrane, while DPH mostly interacts with highly hydrophobic lipid phases of mitochondrial membrane (Zhang et al. 2011). Reportedly, the fluorescence depolarization is mainly due to the rotational diffusion of probe during the excited lifetime. Thus, a high polarization value suggests high structural order or low membrane fluidity of the mitochondrial membrane.

As shown in Fig. 6a, the DPH or HP anisotropy is continuously monitored using Spectrofluorimeter. The results indicate that RQDs induces an obvious decrease in HP anisotropy from 0.35 to 0.25. In contrast, there is no obvious change in DPH anisotropy. However, the anisotropy value of HP increases from 0.35 to 0.44 after the addition of Cadmium ion ( $32 \mu\text{mol}\cdot\text{L}^{-1}$ ). In Fig. 6b, our results also demonstrate that a size-dependent decrease in membrane fluidity of mitochondria is produced by QDs.

### Interaction Sites of QDs on Mitochondria

We investigated the inhibition of CsA, HSA, and EDTA on the QD-induced swelling of mitochondria. As shown in Fig. 7a, CsA, a classical inhibitor of MPT (Halestrap et al. 1997), markedly relieves the swelling of mitochondria, thus identifying the existence of MPT results from the addition of RQDs. HSA is the most abundant protein in human blood plasma and have no obvious inhibition on MPT. In our previous paper, we have demonstrated that HSA will adsorb on QDs surface (Lai et al. 2012). The adsorption behavior of serum proteins will possibly inhibit the interaction of QDs with membrane protein of mitochondria. Therefore, we further clarify the inhibition of HSA on MPT.  $4 \mu\text{mol}\cdot\text{L}^{-1}$  of HSA solution was added into the QDs solution, and then incubated for 2 h. As shown in Fig. 7a, when QDs are pretreated with HSA, the mitochondrial swelling is obviously relieved. EDTA, one of the most prominent chelating agents, is used to bind metal

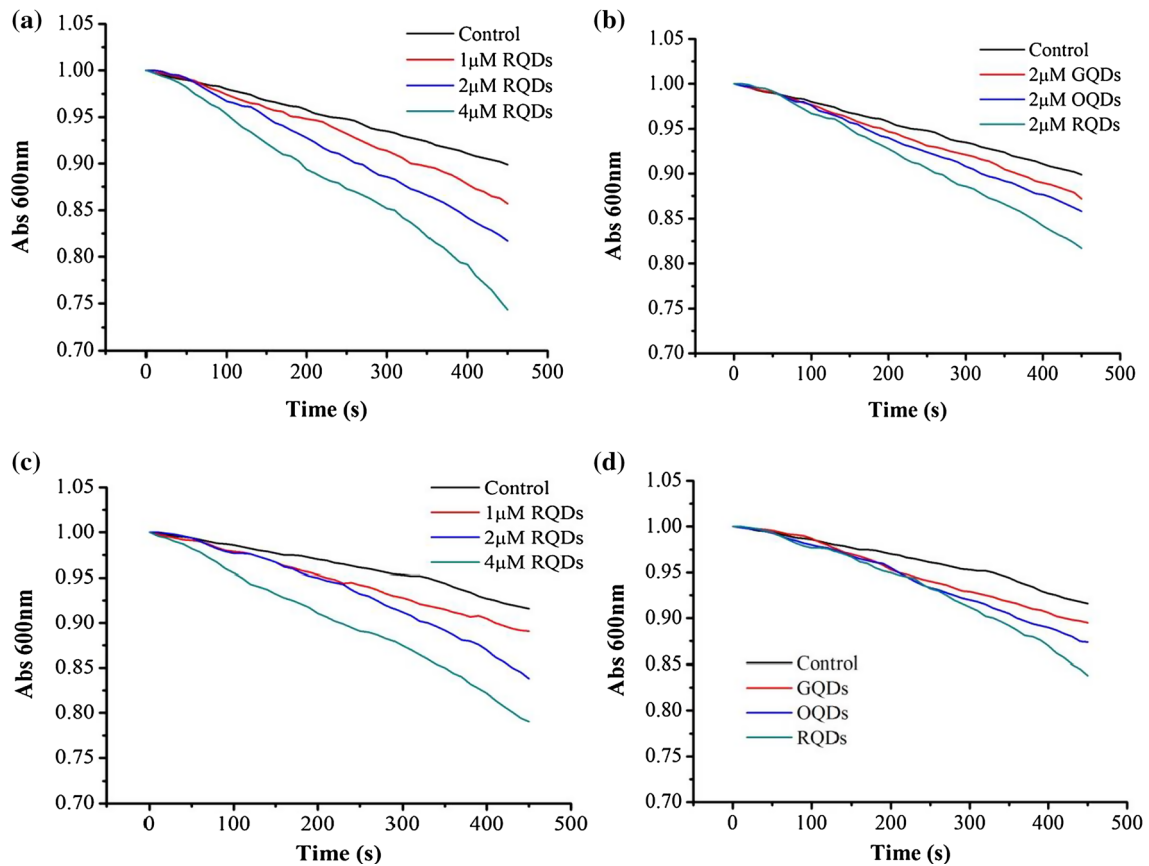


**Fig. 5** Effects of QDs on the permeabilization to  $H^+$  (a, b) and  $K^+$  (c, d) by mitochondrial inner membrane. **a** Mitochondria followed by addition of RQDs: 0, 1, 2, 4  $\mu\text{mol}\cdot\text{L}^{-1}$ . **b** Mitochondria followed by addition of differently sized QDs: GQDs, OQDs and RQDs. **c** Mitochondria followed by addition of RQDs: 0, 1, 2, 4  $\mu\text{mol}\cdot\text{L}^{-1}$ .

**d** Mitochondria followed by addition of differently sized QDs: GQDs, OQDs and RQDs. These experiments were performed using four independent experiments with different mitochondria preparations. The mean values and *standard errors* are shown in Figs. S5–S8

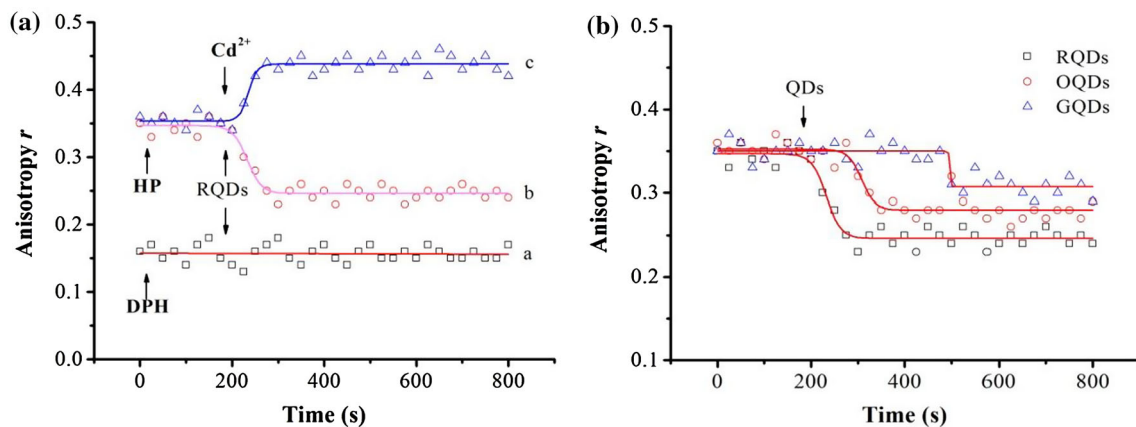


**Fig. 6** Effects of QDs on the membrane fluidity of mitochondria. **a** Time courses of the anisotropic changes of DPH-labeled (curve a) and HP-labeled (curve b) mitochondria followed by addition of 2  $\mu\text{mol}\cdot\text{L}^{-1}$  RQDs and 32  $\mu\text{mol}\cdot\text{L}^{-1}$   $Cd^{2+}$  (curve c). **b** HP-labeled mitochondria followed by addition of 2  $\mu\text{mol}\cdot\text{L}^{-1}$  differently sized

GSH-CdTe QDs: GQDs, OQDs and RQDs. These experiments were performed using four independent experiments with different mitochondria preparations. The mean values and *standard errors* are shown in Fig. S9

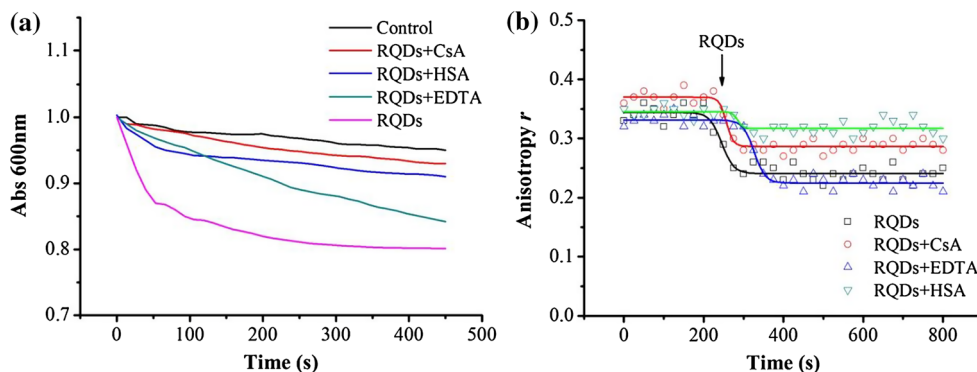


**Fig. 7** Effects of CsA, HSA, and EDTA on mitochondrial swelling (a) and the change of membrane fluidity (b) induced by RQDs (2  $\mu\text{M}$ ). Mitochondria suspension incubated with 0.1mM of different inhibitors (CsA, HSA and EDTA) before measuring. These

experiments were performed using four independent experiments with different mitochondria preparations. The mean values and standard errors are shown in Figs. S10 and S11

ions. Zhang et al. reported that liver mitochondria are able to recover functions after the removal of cadmium ion by EDTA (Zhang et al. 2011). We pretreated mitochondria with EDTA, and then monitored the QD-induced mitochondrial swelling. As shown in Fig. 7a, when the concentration of QDs is 2  $\mu\text{mol}\cdot\text{L}^{-1}$ , EDTA is ineffective at inhibiting the mitochondrial swelling induced by QDs.

We also examined the influence of CsA, HSA, and EDTA on the membrane fluidity of mitochondria. The change in membrane fluidity induced by GQDs is suppressed after pretreatment with 0.1 mM HSA, whereas the pretreatment of CsA and EDTA have no or little effect on the fluidity change of mitochondrial membrane.

### Interaction of QDs with DPPC Model Membranes

Results of fluorescent anisotropy indicate that QDs induce an obvious change in the fluidity of protein regions of mitochondrial membranes, whereas the fluidity of lipid regions is not obviously affected. Moreover, the protective effects of HSA further suggest that the pore-forming protein is probably the interaction site of QDs on mitochondria. To verify the above-mentioned hypothesis, we monitor the interaction between RQDs and model membranes (DPPC) using differential scanning calorimetry and isothermal titration microcalorimetry. Figure 8 shows the differential scanning for mixtures of DPPC suspensions with RQDs. The main phase transition temperature of DPPC exhibits no obvious change when the RQDs concentration is up to 2  $\mu\text{M}$ .

Calorimetric curves for the addition of DPPC suspension (20  $\mu\text{M}$ ) or HSA solution (20  $\mu\text{M}$ ) to RQDs solution (1  $\mu\text{M}$ ) at 298.15 K are shown in Fig. S12. The interaction of HSA solution with RQDs is an exothermic process. However, the thermal power is negligible when DPPC suspension is titrated into the RQDs solution.

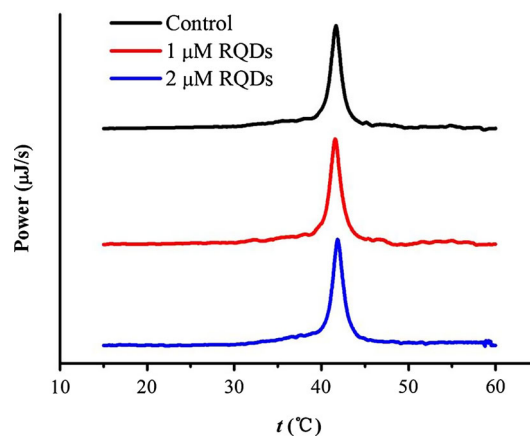


**Fig. 8** Calorimetric scans for mixture of DPPC with different concentrations of GQDs. The heating rate was 1  $^{\circ}\text{C}/\text{min}$  from 10 to 70  $^{\circ}\text{C}$

### Discussion

This study clarifies the toxicological effect of CdTe QDs of different sizes on mitochondria. Our previous study has demonstrated that QDs can enter cells via the clathrin-mediated endocytic processes, further leading to cell apoptosis or necrosis (Lai et al. 2015b). Moreover, we now know that mitochondria play a key role in cell apoptosis, necrosis, or autophagy. Thus, the observed results lead us to explore the potential role of mitochondria in QD toxicity (Li et al. 2011).

MPT represents an increase in permeability of the mitochondrial inner membranes (Bernardi et al. 1992). Pioneering studies demonstrated that MPT was the result of the opening of a non-specific MPT pore (MPTP). The MPTP is a protein pore that spans both the mitochondrial inner and outer membranes (Kobayashi et al. 2003). MPTP opening can induce mitochondrial swelling, membrane depolarization, uncoupling of oxidative phosphorylation, and so on.



To ascertain whether the addition of QDs causes the mitochondrial permeability transition, the direct effects of QDs of different sizes on mitochondria isolated from rat liver were examined. Results of flow cytometry indicate that GSH-CdTe QDs induce a reduction in mitochondrial membrane potential (Fig. 3). Meanwhile, GSH-CdTe QDs cause an obvious swelling of mitochondria (Fig. 4). In addition, a remarkable change in the fluidity of mitochondrial membrane is observed, which results from the increase in membrane permeability (Passarella et al. 2003). These results demonstrate that CdTe QDs can trigger MPT. With increasing QDs size, a pronounced mitochondrial swelling and depolarization is observed.

When dispersed in the mitochondrial suspension, QDs are prone to interact with mitochondrial membrane. In order to clarify the mechanism of mitochondrial toxicity, we focus on the interaction of QDs with mitochondrial membrane. The change in mitochondrial membrane fluidity was examined using two classical probes, HP and DPH. HP mainly accumulates in polar regions or associates with proteins in the mitochondrial membrane, while DPH mostly interacts with highly hydrophobic lipid phases of mitochondrial membrane. An obvious decrease in the HP anisotropy is observed after treatment with QDs, whereas no obvious change in the DPH anisotropy is observed. Since HP preferentially binds with proteins of mitochondrial membrane, we suggest that the HP anisotropy change results from the conformational change of pore-forming proteins involved in MPTP formation. However, the addition of Cadmium ion induces an obvious increase of the HP anisotropy, which is different from the effects induced by QDs.

The inhibition of EDTA on MPT was also investigated. Most published research findings have shown that the toxicological mechanism of QDs is related to the release of  $\text{Cd}^{2+}$ . Figure 7a shows the addition of EDTA only partially inhibits the QD-induced mitochondrial swelling. Moreover, the changes induced by QDs and Cadmium ion in the fluidity of mitochondrial membrane are different (Fig. 6a). Therefore, the mechanism by which QDs and Cadmium ion induce mitochondrial toxicity is different. It is proposed that the interaction of QDs with membrane protein plays a key role in mitochondrial toxicity.

To confirm this speculation, we investigated the protection by HSA in QD-induced mitochondrial dysfunction. The adsorption behavior of serum proteins will possibly inhibit the interaction of QDs with membrane protein of mitochondria. As shown in Fig. 7a, when QDs are pretreated with HSA, the mitochondrial swelling is obviously relieved. Moreover, the change of membrane fluidity induced by QDs is suppressed after pretreatment with 0.1 mM HSA. Consequently, the mitochondrial toxicity

may result from the interaction of QDs with membrane protein involved in the MPTP formation. The phospholipid-to-protein ratio of outer mitochondrial membrane is about 1:1 by weight, which is similar to that of eukaryotic plasma membrane. The interaction of QDs with model membranes and proteins was examined using differential scanning calorimetry and isothermal titration microcalorimetry. As shown in Fig. 8, the width and maximum temperature of the main phase transition of DPPC show no obvious change when the RQDs concentration is up to 2  $\mu\text{M}$ . Moreover, the calorimetric curves in Fig. S12 indicate the thermal power is negligible when DPPC suspension is titrated into the RQDs solution. Therefore, the binding affinity of RQDs with protein is higher than phospholipid. Due to the small size, QDs possess high surface energy, and thus are extremely reactive (Deng et al. 2012). Moreover, with increasing QDs size, the surface area of QDs at the same molar concentration increases, thus the binding constants of QDs to membrane protein will increase. On the basis of these analyses, a size-dependent mitochondrial toxicity of QDs is reasonable.

## Conclusion

In conclusion, the mitochondrial toxicity induced by GSH-CdTe QDs of different sizes was investigated for the first time in this report. Results of spectroscopic and microscopic studies show that QDs induce MPT, which results in mitochondrial swelling, membrane potential collapse, membrane permeability to  $\text{H}^+$  and  $\text{K}^+$ , change in the fluidity of membrane, and alterations of mitochondrial ultrastructure. Moreover, a size-dependent mitochondrial toxicity of QDs was observed. The difference between the membrane fluidity induced by QDs and Cadmium ion and the ineffective protective effects of EDTA suggests that the mitochondrial toxicity of QDs cannot be only attributed to the release of metal ion. The protective effects of HSA indicate that the interaction of QDs with pore-forming protein gives rise to the increase in membrane fluidity. Results of the interaction of QDs with model membranes and proteins using differential scanning calorimetry and isothermal titration microcalorimetry also demonstrate that the binding affinity of QDs with protein is higher than phospholipid. On basis of these results, the toxicological mechanism of CdTe QDs, which involves the interaction of QDs with membrane protein, is proposed.

**Acknowledgments** The authors gratefully acknowledge the financial support from the National Science Fund for Distinguished Young Scholars of China (Grant No. 21225313) and National Natural Science Foundation of China (Grant Nos. 21403017, 21473125).

## References

- Balaban RS, Nemoto S, Finkel T (2005) Mitochondria, oxidants, and aging. *Cell* 120:483–495
- Bernardi P, Vassanelli S, Veronese P, Colonna R, Szabo I, Zoratti M (1992) Modulation of the mitochondrial permeability transition pore. Effect of protons and divalent cations. *J Biol Chem* 267:2934–2939
- Chen N, He Y, Su YY, Li XM, Huang Q, Wang HF, Zhang XZ, Tai RZ, Fan CH (2012) The cytotoxicity of cadmium-based quantum dots. *Biomaterials* 33:1238–1244
- Choi B, Hwang S, Kim I, Shin H, Kim Y, Kim E (1998) Fabrication and room-temperature characterization of a silicon self-assembled quantum-dot transistor. *Appl Phys Lett* 73:3129–3131
- Cossarizza A, Baccaricontri M, Kalashnikova G, Franceschi C (1993) A new method for the cytofluorometric analysis of mitochondrial membrane potential using the J-aggregate forming lipophilic cation 5, 5', 6, 6'-tetrachloro-1, 1', 3, 3'-tetraethylbenzimidazolcarbocyanine iodide (JC-1). *Biochem Biophys Res Commun* 197:40–45
- Deng ZJ, Liang MT, Toth I, Monteiro M, Minchin RF (2012) Plasma protein binding of positively and negatively charged polymer-coated gold nanoparticles elicits different biological responses. *Nanotoxicology* 7:314–322
- Eliseev P, Li H, Stintz A, Liu G, Newell T, Malloy K, Lester L (2000) Transition dipole moment of InAs/InGaAs quantum dots from experiments on ultralow-threshold laser diodes. *Appl Phys Lett* 77:262–264
- Fernandes MA, Custodio JB, Santos MS, Moreno AJ, Vicente JA (2006) Tetrandrine concentrations not affecting oxidative phosphorylation protect rat liver mitochondria from oxidative stress. *Mitochondrion* 6:176–185
- Halestrap AP, Connern CP, Griffiths EJ, Kerr PM (1997) Cyclosporin a binding to mitochondrial cyclophilin inhibits the permeability transition pore and protects hearts from ischaemia/reperfusion injury. *Detection of Mitochondrial Diseases*, Springer US, pp 167–172
- Hardman R (2006) A toxicologic review of quantum dots: toxicity depends on physicochemical and environmental factors. *Environ Health Perspect* 4(2):165–172
- Kim JS, He L, Lemasters JJ (2003) Mitochondrial permeability transition: a common pathway to necrosis and apoptosis. *Biochem Biophys Res Commun* 304:463–470
- Kim S, Lim YT, Soltesz EG, De Grand AM, Lee J, Nakayama A, Parker JA, Mihaljevic T, Laurence RG, Dor DM (2004) Near-infrared fluorescent type II quantum dots for sentinel lymph node mapping. *Nat Biotechnol* 22:93–97
- Kobayashi T, Kuroda S, Tada M, Houkin K, Iwasaki Y, Abe H (2003) Calcium-induced mitochondrial swelling and cytochrome c release in the brain: its biochemical characteristics and implication in ischemic neuronal injury. *Brain Res* 960:62–70
- Kowaltowski AJ, Castilho RF, Vercesi AE (2001) Mitochondrial permeability transition and oxidative stress. *FEBS Lett* 495:12–15
- Lai L, Lin C, Xu ZQ, Han XL, Tian FF, Mei P, Li DW, Ge YS, Jiang FL, Zhang YZ (2012) Spectroscopic studies on the interactions between CdTe quantum dots coated with different ligands and human serum albumin. *Spectrochim Acta Part A* 97:366–376
- Lai L, Jin JC, Xu ZQ, Ge YS, Jiang FL, Liu Y (2015a) Spectroscopic and microscopic studies on the mechanism of mitochondrial toxicity induced by CdTe QDs modified with different ligands. *J Membran Biol* 248(4):1–14
- Lai L, Jin JC, Xu ZQ, Mei P, Jiang FL, Liu Y (2015b) Necrotic cell death induced by the protein-mediated intercellular uptake of CdTe quantum dots. *Chemosphere* 135:240–249
- Lemasters JJ, Theruvath TP, Zhong Z, Nieminen AL (2009) Mitochondrial calcium and the permeability transition in cell death. *Biochimica et Biophysica Acta (BBA)-Bioenergetics* 1787:1395–1401
- Leutwyler WK, Bürgi SL, Burgl H (1996) Semiconductor clusters, nanocrystals, and quantum dots. *Science* 271:933–937
- Li JH, Zhang Y, Xiao Q, Tian FF, Liu XR, Li R, Zhao GY, Jiang FL, Liu Y (2011) Mitochondria as target of quantum dots toxicity. *J Hazard Mater* 194:440–444
- Liu W, Wu Y, Wang C, Li HC, Wang T, Liao CY, Cui L, Zhou QF, Yan B, Jiang GB (2010) Impact of silver nanoparticles on human cells: effect of particle size. *Nanotoxicology* 4:319–330
- Liu XR, Li JH, Zhang Y, Ge YS, Tian FF, Dai J, Jiang FL, Liu Y (2011) Mitochondrial permeability transition induced by different concentrations of zinc. *J Membran Biol* 244:105–112
- Loss D, DiVincenzo DP (1998) Quantum computation with quantum dots. *Phys Rev A* 57:120
- Michalet X, Pinaud FF, Bentolila LA, Tsay JM, Doose S, Li JJ, Sundaresan G, Wu AM, Gambhir SS, Weiss S (2005) Quantum dots for live cells, in vivo imaging, and diagnostics. *Science* 307:538–544
- Nalika N, Parvez S (2015) Mitochondrial dysfunction in titanium dioxide nanoparticle-induced neurotoxicity. *Toxicol Mech Method* 25(5):1–9
- Passarella S, Atlante A, Valenti D, de Bari L (2003) The role of mitochondrial transport in energy metabolism. *Mitochondrion* 2:319–343
- Petronilli V, Šileikytė J, Zulian A, Dabbeni-Sala F, Jori G, Gobbo S, Tognon G, Nikolov P, Bernardi P, Ricchelli F (2009) Switch from inhibition to activation of the mitochondrial permeability transition during hematoporphyrin-mediated photooxidative stress. Unmasking pore-regulating external thiols. *Biochimica et Biophysica Acta* 1787:897–904
- Piao MJ, Kang KA, Lee IK, Kim HS, Kim S, Choi JY, Choi J, Hyun JW (2011) Silver nanoparticles induce oxidative cell damage in human liver cells through inhibition of reduced glutathione and induction of mitochondria-involved apoptosis. *Toxicol Lett* 201:92–100
- Raffaella RP, Castro SL, Hepp AF, Bailey SG (2002) Quantum dot solar cells. *Prog Photovoltaics Res Appl* 10:433–439
- Ricchelli F, Jori G, Gobbo S, Nikolov P, Petronilli V (2005) Discrimination between two steps in the mitochondrial permeability transition process. *Int J Biochem Cell Biol* 37:1858–1868
- Schleh C, Semmler-Behnke M, Lipka J, Wenk A, Hirn S, Schäffler M, Schmid G, Simon U, Kreyling WG (2012) Size and surface charge of gold nanoparticles determine absorption across intestinal barriers and accumulation in secondary target organs after oral administration. *Nanotoxicology* 6:36–46
- Sharma V, Anderson D, Dhawan A (2012) Zinc oxide nanoparticles induce oxidative DNA damage and ROS-triggered mitochondria mediated apoptosis in human liver cells (HepG2). *Apoptosis* 17:852–870
- Son DI, Kwon BW, Park DH, Seo W-S, Yi Y, Angadi B, Lee C-L, Choi WK (2012) Emissive ZnO-graphene quantum dots for white-light-emitting diodes. *Nat Nanotechnol* 7:465–471
- Su Y, He Y, Lu H, Sai L, Li Q, Li W, Wang L, Shen P, Huang Q, Fan C (2009) The cytotoxicity of cadmium based, aqueous phase-synthesized, quantum dots and its modulation by surface coating. *Biomaterials* 30:19–25
- Unfried K, Albrecht C, Klotz L-O, Von Mikecz A, Grether-Beck S, Schins RP (2007) Cellular responses to nanoparticles: target structures and mechanisms. *Nanotoxicology* 1:52–71
- Werlin R, Priester JH, Mielke RE, Krämer S, Jackson S, Stoimenov PK, Stucky GD, Cherr GN, Orias E, Holden PA (2011) Biomagnification of cadmium selenide quantum dots in a simple experimental microbial food chain. *Nat Nanotechnol* 6:65–71

- Xiao JB, Kai GY, Chen XQ (2012) Effect of CdTe QDs on the protein-drug interactions. *Nanotoxicology* 6:304–314
- Xin LL, Wang JS, Fan GQ, Che BZ, Wu YH, Guo SF, Tong J (2015) Oxidative stress and mitochondrial injury-mediated cytotoxicity induced by silver nanoparticles in human A549 and HepG2 cells. *Environ Toxicol*
- Yang YJ, Lan JF, Xu ZG, Chen T, Zhao T, Cheng T, Shen JM, Lv SY, Zhang HX (2014) Toxicity and biodistribution of aqueous synthesized ZnS and ZnO quantum dots in mice. *Nanotoxicology* 8:107–116
- Zhang Y, Li JH, Liu XR, Jiang FL, Tian FF, Liu Y (2011) Spectroscopic and microscopic studies on the mechanisms of mitochondrial toxicity induced by different concentrations of cadmium. *J Membran Biol* 241:39–49